Exp. Theo. NANOTECHNOLOGY 10 (2026) 109-121 https://doi.org/10.56053/10.1.109

Experimental and finite element analysis of porous functionally graded blend (PLA\UHMWPE/PVA)

Enas al-Zubaidy[1,*], *Ahmed Fadhil Hamza*[1], *Zuhair Jabbar Abdul Ameer*[2]

[1]Department of Engineering of Polymer and Petrochemical Industries, College of Materials Engineering, University of Babylon, Hillah, Iraq
[2]Department of Prosthetics and Orthotics, College of Engineering, University of Karbala, Karbala, Iraq
[*]) Email: enas_talib@hilla.unc.edu.iq

Received 1/10/2025, *Received in revised form* 12/11/2025, *Accepted* 21/11/2025, *Published* 15/1/2026

To simulate the structure of living tissues and find alternatives with similar properties, and to reduce the differences between orthopedic and hip implants, functional grading is used to fabricate artificial replacements for a part of the knee joint, study their mechanical properties, and analyze the results using the finite element method. Functionally graded blends (10%-50% wt. PLA)/ (90%-50% wt. UHMWPE)/ 50% wt. PVA) are used. A porous implant is chosen instead of a solid one to reduce the stress-shielding effect. Finite element analysis (FEA) is used to analyze the stress-shielding effect of FGB under the loads acting on porous hip implants as an alternative to dense stems. Hardness and tensile tests are performed to analyze the behavior of functionally graded blend samples and a functionally graded porous hip implant model under critical loads, and are analyzed using a digital microscope to determine the count and average pore size. The implant design is found to be sensitive to the functional grading factor . Under tensile conditions, when the prosthetic leg model (PFGBs) structure takes a gradient according to stiffness values from the lowest (39.08) to the highest (46.9), dislocation and loosening are observed at the maximum tensile force at a displacement of (50 mm) for the highest total deformation of (16.564 mm) and the maximum von Mises stress of (12.736 MPa). While the prosthetic leg model under tension, when the (PFGBs) structure takes a gradient according to stiffness values from the highest (46.9) to the lowest (39.08), dislocation and loosening occur at the maximum tensile force and at the point of contact of the ball head with the leg under tensile loading conditions at a displacement of (50 mm) for the highest total deformation of (18.904 mm) and the maximum von Mises stress of (22.559 MPa).

Keywords: FGBs; FEM; Femoral stem Prosthesis.

1. INTRODUCTION

Functional gradients are key in living tissues, and nanotechnology enables precise control of implant composition at the nanoscale. This allows optimization of mechanical strength and biocompatibility, closely mimicking natural tissue structure [1]. However, biocompatibility evaluation of the biological response of FGBs made of hydroxyapatite and polymer matrices suggests that the optimized FGBs promote better cell adhesion and proliferation compared to conventional homogeneous materials [2]. There are solutions to the causes of aseptic loosening, the most significant of which are the impact of residual particles due to wear, pressure protection, and, finally, micro-movements. Given that such problems occur approximately 15 years after surgery, it is necessary to design a prosthetic system that simultaneously enhances the biomechanical interaction between the prosthesis and the bone, while simultaneously reducing the pressure on the surrounding tissues[3] . The development of a synthetic, high-density polyvinyl chloride (HMWPEU) gradient-structured biomaterial produced improved in vivo growth healing mechanisms [4].

When it comes to the use of porosity in design, it has been observed to have a negative impact on mechanical properties such as stiffness and strength, while providing superior performance in other areas such as vibration reduction, thermal insulation, energy absorption and dissipation, etc., making it suitable for medical and engineering applications. In addition to its direct impact on natural frequencies [5], the bone adaptation around the graft is a problem, and radial gradation using a low-stiffness material in the outer layer has a significant impact on the bone adaptation process [6]. Although previous literature has focused on conventional homogeneous-structured prostheses, the functional adaptation and practical application of porous mesh prostheses on the host bone need to be investigated. Compared with conventional homogeneous-structured prostheses, functionally graded mesh prostheses have an optimal stress distribution with superior mechanical and biological properties [7]. Challenge the variations between native tissues as complex materials (porosity, mineralization, and fiber alignment) to achieve suitable replacements by mimicking the gradients in heterogeneous tissues to influence strength, plasticity, and cell signaling [8]. Gradients also include signals, as cell migration has been observed in response to gradients of soluble chemo attractants, surface-bound molecules, and stiffness [9].The most studied factors in relation to cell gradients are (structure, porosity, stiffness, and biochemical concentration). While scaffolds are often used for soft tissues, hydrogels for more flexible materials, and rigid polymers and ceramics as alternatives for hard tissues due to their slow absorption and ability to withstand high mechanical loads [10].

This study evaluates the feasibility of using functionally graded bio-composites (FGBPs) for prosthetic limb stems. It investigates the deformation mechanisms of the constituent materials experimentally and via finite element simulations, and analytically examines the tensile behavior of the spherical head and stem, providing insights into their structural performance.

2. EXPERIMENTAL

2.1 Materials

The matrix phase is ultra-high molecular weight polyethylene (UHMWPE) in the form of white granules, with a molecular weight below 1,700,000, supplied by LOBA CHEME PVT.LTD. The second phase is poly lactic acid (PLA) (98% purity) in the form of a white powder, at 151°C, supplied by BASF 3D Printing Solutions BV. Poly vinyl alcohol (PVA) is added to matrix to obtain a porous structure (appearance of PVA: white powder, molecular weight (1,700-1,800) originating in Germany, packed in the UK by ME Scientific Engineering LTD.

2.2 Preparation (FGB)

The powder technology theory is used to prepare functionally graded samples as well as porous graded samples by mixing powders (poly lactic acid with ultra-high molecular weight polyethylene) in the solid state at the volume fractions shown in Table (1). Porous samples are also prepared with the same volume fraction gradient shown in Table (2).

Table 1 FGB compositions.

Samples	PLA wt. %	UHMWPE wt. %
PLA\UHMWPE1	10	90
PLA\UHMWPE2	20	80
PLA\UHMWPE3	30	70
PLA\UHMWPE4	40	60
PLA\UHMWPE5	50	50

Table 2 PFGB compositions.

Samples	PLA wt. %	UHMWPE wt. %	PVA wt.%
PLA\UHMWPE\PVA1	9	81	10
PLA\UHMWPE\PVA2	16	64	20
PLA\UHMWPE\PVA3	21	49	30
PLA\UHMWPE\PVA4	24	36	40
PLA\UHMWPE\PVA5	25	25	50

Poly lactic acid is mixed with ultra-high molecular weight polyethylene in powder form at the weight ratios calculated in Table (1) and pressed into a mold measuring (185 mm x 195 mm and 4 mm deep, assuming a 1 mm mold tolerance), Figure (1, a). The samples are pressed into the mold in a heat press at a pressure of 5 MPa and a temperature of 175 °C and gradually cooled to room temperature. Poly vinyl alcohol (PVA) is added in the liquid state (the solution is added in a ratio of 100 g of deionized water: 10 g of polyvinyl alcohol). The mixture is continuously mixed by mechanical stirrer to ensure the homogeneity of the mixture for 10 minutes and gradually cooled to room temperature. It is worth noting that powder technology requires a heating temperature of up to 185°C with increasing volume fraction of PLA and vice versa, as the volume fraction decreases (from PLA\UHMWPE1 to PLA\UHMWPE2) the heating temperature reaches 175 °C. The experimental work involved the fabrication of six different samples (FGBs and PFGBs) using powder technology, Figure (1, b, c).

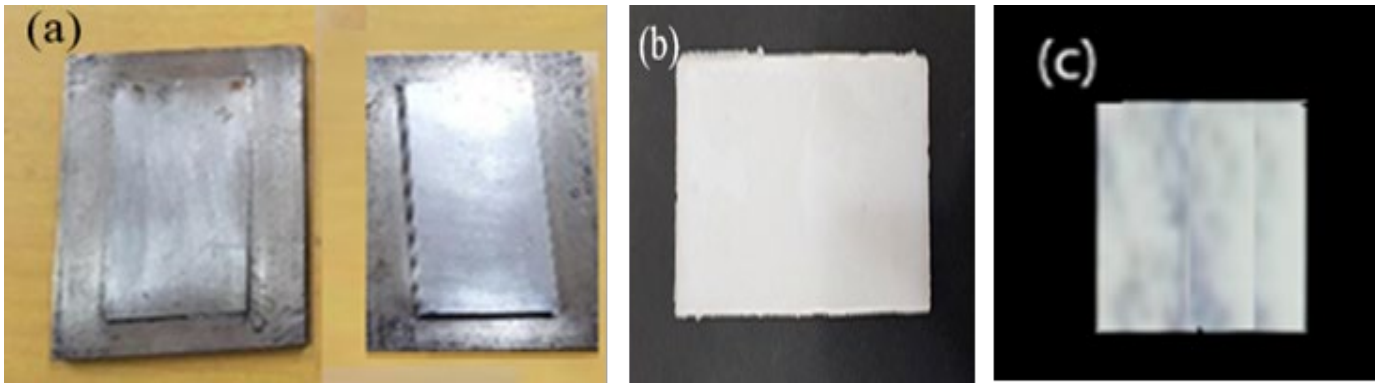

Figure 1 (a) the Steel Mold (b) The Sheet of FGBs, and (c) The Sheet of PFGBs.

2.3 Methods

2.3.1 Mechanical hardness test for blends properties of FGBs & PFGBs

Mechanical hardness test for blends properties of FGBs & PFGBs (20 mm width, 30 mm length, 3 mm thickness) are tested using a Shore D hardness tester (TH 210 FJ), made in Germany according to ASTM D2240 [11], which is required to measure the flexural strength of the material. A needle is placed perpendicular to the specimen to obtain accurate readings. The specimen surface had to be smooth and clean, (Figure 2, a, b). Each specimen is tested five times at different positions on the specimen simultaneously. It is observed that the final hardness values of the specimens depended significantly on the volume fraction, Figure (3, a, b).

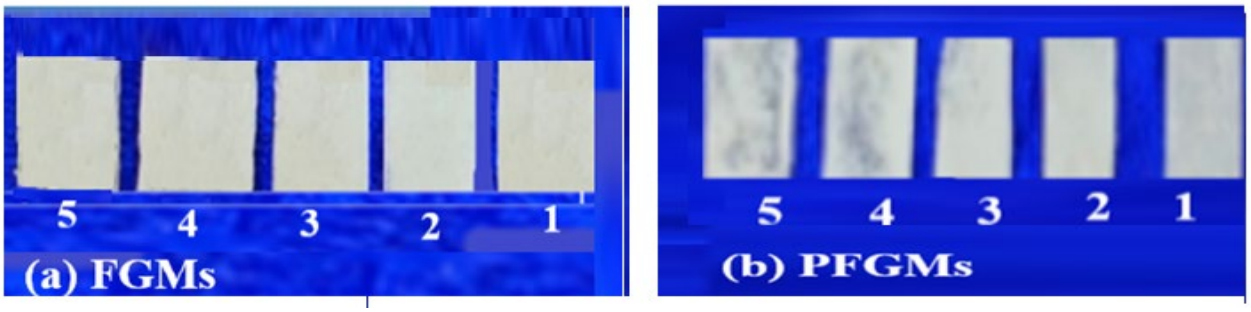

Figure 2 Hardness samples for PFGB's Composite Materials.

Figure (3, a) shows the processing characteristics of the matrix (PLA: UHMWPE), with fractional volume as in table (1). The maximum stiffness decreases with increasing PLA wt. % loading. The decrease in maximum stiffness values shows that the presence of PLA in the blends tends to reduce the workability and elasticity of the matrix. Mixing Two Polymers phase-separated mixtures are what we get when trying to mix most polymers. But phase-separated materials are often more useful. These mixtures are called immiscible mixtures. Polyvinyl alcohol is immiscible with UHMWPE. Instead, the polyvinyl acid will separate from the UHMWPE into small clumps. Under an electron microscope, the small clumps of UHMWPE make a big difference to the material. It is a fairly brittle material, hard and brittle. However, the clumps are elastic and can absorb energy under stress. This prevents the polyvinyl acid from breaking. This immiscible mixture has a greater ability to stretch rather than break than regular polyvinyl acid, meaning it is more rigid and flexible [12].

Figure (3, b) shows the processing properties of the matrix (PLA: UHMWPE: PVA), with the fractional size as shown in Table 2. The decrease in maximum hardness values shows that the presence of PVA in the blends tends to reduce the hardness values of the matrix. The ratio (21 wt. % PLA: 49 wt. %: UHMWPE: 30 wt. % PVA) has the highest value. One of the most important ways to create a strong, immiscible blend is to use approximately equal amounts of the two polymers. When the relative amounts of the two polymers are approximately equal, we obtain a different morphology than when one of them is significantly excess; they form two continuous phases. This means that both phases will bear the burden of any stress on the material, making it stronger [13].

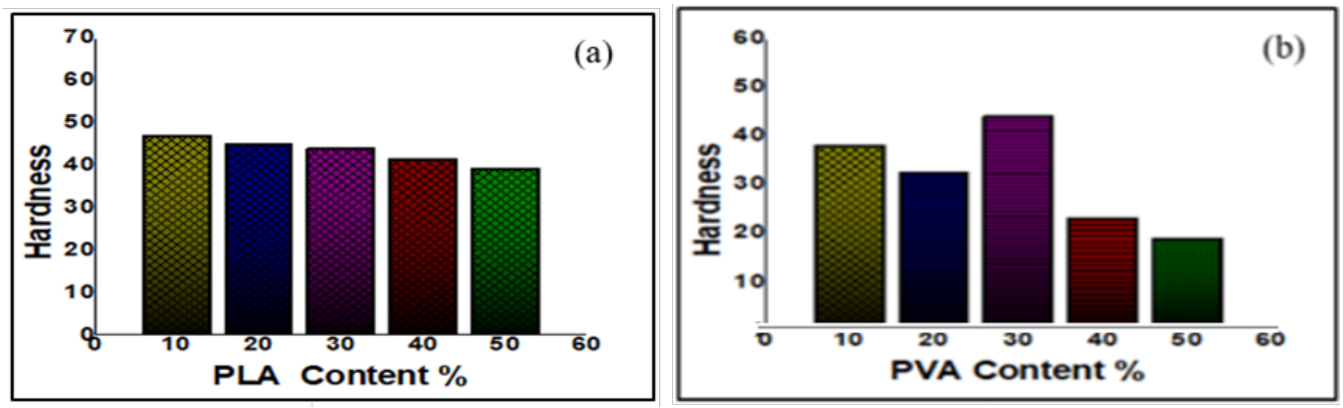

Figure 3 Hardness data analysis chart for (a) FGBs, and (b) PFGBs.

Figure (4) Shows the digital microscopic images of PFGBs. Microscopic images are taken by a digital microscope and the total count pores and average pore size are calculated using ImageJ software. Table (3) shows the pore count and average pore size for each layer. It is noted that the highest value for the count pores is for the mixture (PLA\UHMWPE\PVA 5) and therefore it is used as a surface layer for the artificial prosthetic structure. The addition of PVA reduces the mechanical properties of the mixture and textures the matrix due to its hydrophilic properties and biodegradability, making it more suitable for medical engineering applications.

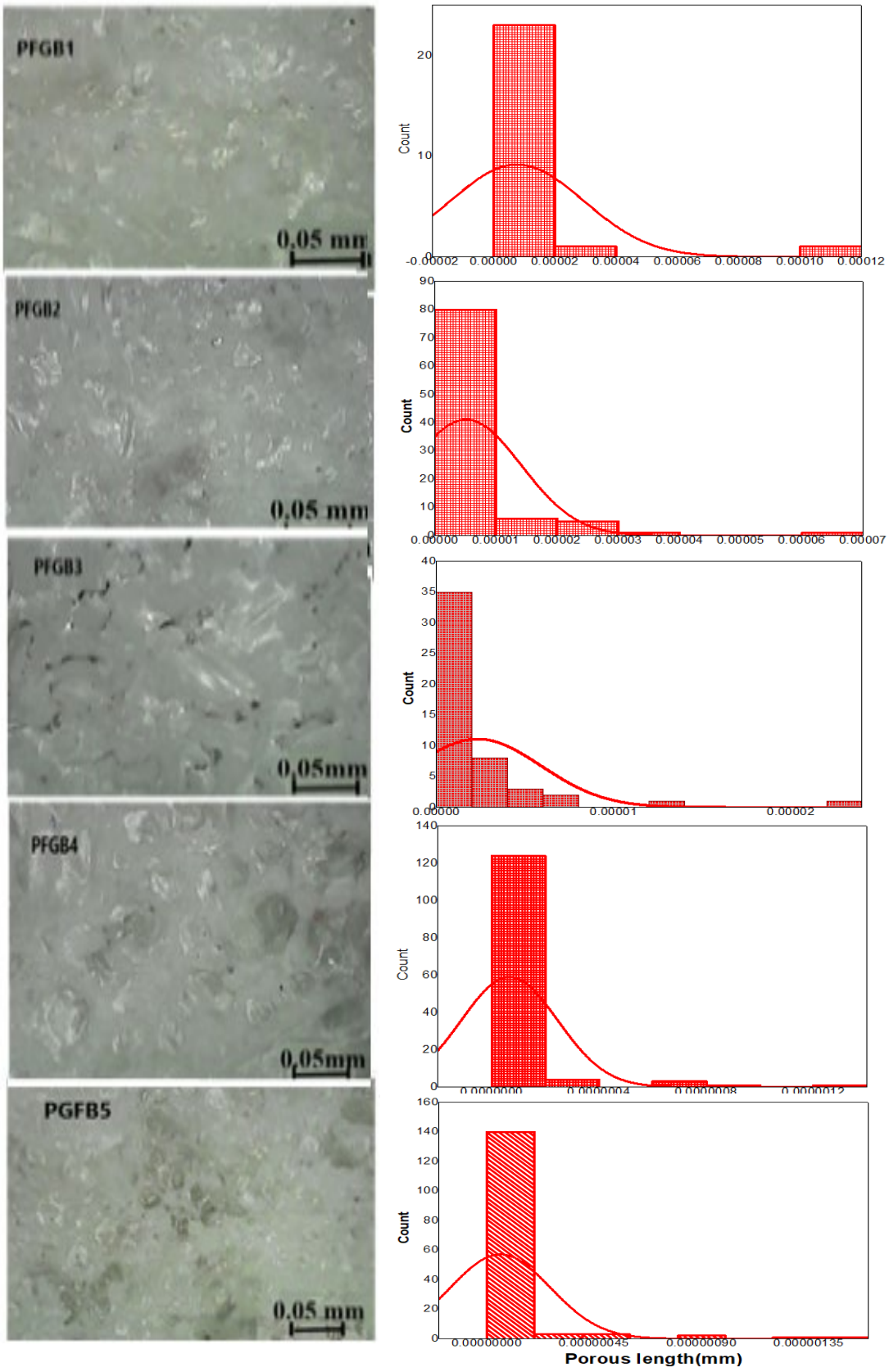

Figure 4 Illustration of Digital Microscopic Images for PFGBs with their standard deviation.

Table 3 PFGB compositions.

Samples	Pores Count	Average Size
PLA\UHMWPE\PVA 1	86	9.773E-6
PLA\UHMWPE\PVA 2	95	5.347E-6
PLA\UHMWPE\PVA 3	50	2.511E-6
PLA\UHMWPE\PVA 4	127	5.122E-6
PLA\UHMWPE\PVA 5	157	1.676E-6

2.3.2 Strength measurement of FGBs & PFGBs for tension test

Figure (5), a tensile test specimens is cut from a functionally graded blend sheet as dimensioned in Figure (1, b, c) according to ASTM D638 [14], the test is performed at a speed of 5 mm/min, with the load applied until the specimen fails. Stress–strain data are obtained. Five FGBs and PFGB specimens are tested at a time, and the mechanical properties are calculated based on the average of the five specimens' data.

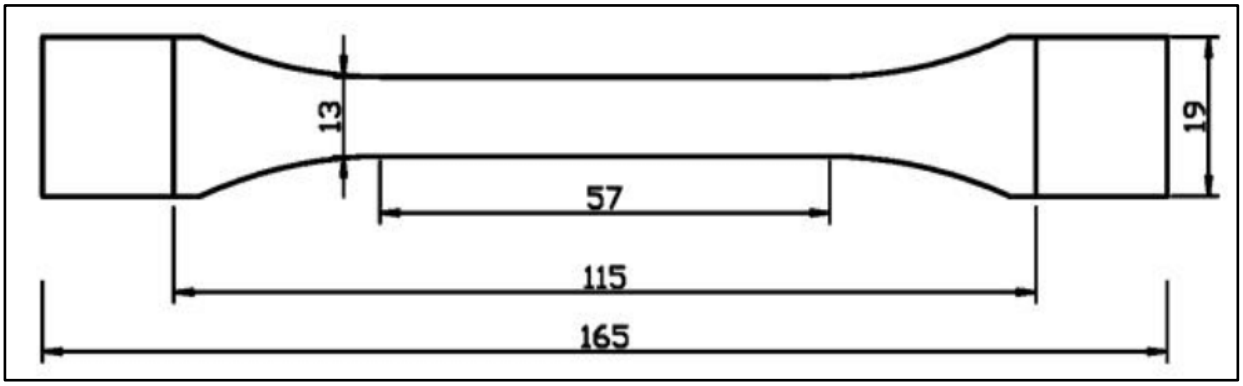

Figure 5 Universal Tensile Test of FGB Composite Materials [14].

Figure (6, a) shows the load-deformation curves for each layer of FGB composites, illustrating the behavior of each layer under tensile load. The effect of phase separation of the two polymers is evident from the observation of the curved trajectory and the gradual decrease in the area under the curve (the plastic region) for all solid samples. Therefore, the graded material generally becomes more elastic and bends more flexibly as the percentage of added poly lactic acid increases and the area under the curve decreases accordingly. For immiscible materials such as poly lactic acid and ultrahigh molecular weight polyethylene, phase separation occurs. At different percentages, the material with a higher volume fraction outperforms the one with a lower volume fraction has been reported that the more elastic component can surround the less elastic component, forming a continuous matrix phase[14,15]. At higher speeds, this may not be achieved, and at lower speeds, the stress may decrease and the distance under the curve may increase, depending on the level of stress distributed among the polymers in the mixture. Nevertheless, the obtained results confirm the results of the hardness test in the paragraph above. This indicator confirms the results of the hardness test in the above paragraph.

Fig. (6,b) shows the load-deformation curves for each layer of PFGB composites, illustrating the behavior of each layer under tensile load. A continuous structure is one in which a continuous secondary phase is interconnected within a continuous matrix. Therefore, considering PLA as a continuous secondary phase allows the continuous structure to produce conductive polymer blends [16,17]. When the secondary phase is patterned, it can be used in tissue engineering scaffolds [18,19]. Therefore, PVA

plays a crucial role in shaping the overall matrix structure, and altering its concentration can transform the matrix phase into a dispersed one. The dispersed phase helps form a structure with stronger properties. However, the area under the curve gradually decreases with varying volume fractions and under varying load conditions, time, and at room temperature.

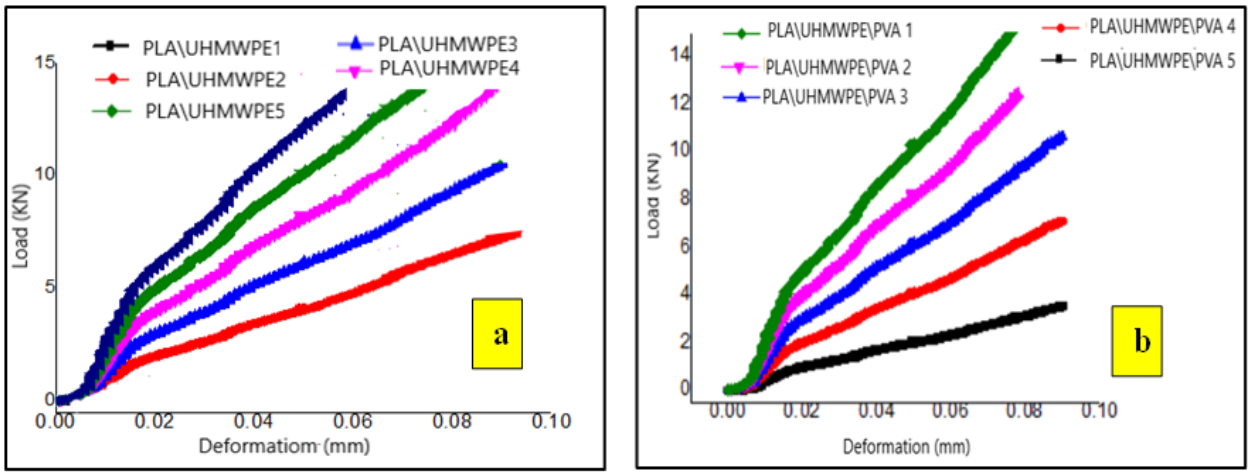

Figure 6 Experimental load–deformation curves from the tension test for (a) FGBs and (b) PFGBs.

2.4 Effective Material Properties

The active material properties of the FGB plate are assumed to change continuously along its thickness direction. These properties are obtained using a simple power law distribution or an exponential law that calculates the volume fraction of each FGB component.

2.4.1 Exponential law

Exponential law of FGB states that ("For a FGB structure of uniform thickness 'h', the material properties 'P(z)' at any point located at 'z' distance from the mid-plane surface is given by [20]:

$$P(z) = P_t e^{\left(-\lambda\left(1-\frac{2z}{h}\right)\right)}, \text{where, } \lambda = \frac{1}{2}\ln\left(\frac{P_t}{P_b}\right) \quad (1)$$

$P(z)$ Refers to material property like Young's modulus of elasticity (E), shear modulus of elasticity (G), Poisson's ratio (υ), and material density (ρ) of the FGB structure. P_t and P_b are material properties at top (z=+h/2) and bottom (z=-h/2) surfaces. λ is material grading indexes which depend on the design requirement.

2.4.2 Power law

The power-law distribution can be written as [21]:

$$V_{PLA}(z) = \left(\frac{z}{h} + \frac{1}{2}\right)^n, \quad V_{UHMWPE}(z) = 1 - V_{PLA}(z) \quad (2)$$

where n is the power law index, $0 \leq n \leq \infty$. The functionally graded two-component material and its properties, such as Young's modulus E and bulk density ρ, are obtained using the following steps[22]:

$$E = (E_{\mathrm{PLA}} - E_{\mathrm{UHMWPE}})\left(\frac{z}{h} + \frac{1}{2}\right)^{n} + E_{\mathrm{UHMWPE}} \quad (3)$$

$$\rho = (\rho_{\mathrm{PLA}} - \rho_{\mathrm{UHMWPE}})\left(\frac{z}{h} + \frac{1}{2}\right)^{n} + \rho_{\mathrm{UHMWPE}} \quad (4)$$

$$\upsilon = (\upsilon_{\mathrm{PLA}} - \upsilon_{\mathrm{UHMWPE}})\left(\frac{z}{h} + \frac{1}{2}\right)^{n} + \upsilon_{\mathrm{UHMWPE}} \quad (5)$$

In the present work, the power-law distribution is used to continuously gradate material properties in the thickness direction. Table (4) illustrates the mechanical properties of FGBSs.

Table 4 The properties of FGBs.

Layers	Blend	Properties		
		Young's modulus E(MPA)	Poison's ratio	Density (g/cm3)
Layers2	PLA\UHMWPE1	49.8	0.352	1.243
Layers3	PLA\UHMWPE2	48.8	0.402	1.215
Layers4	PLA\UHMWPE3	50.4	0.346	1.264
Layers5	PLA\UHMWPE4	49.3	0.358	1.225
Layers6	PLA\UHMWPE5	52.24	0.33	1.328

2.4.3 FGB plate with porosities

Suppose we have a plate assigned a Cartesian coordinate system, x, y, z, where x, y is the mid plane of the plate and z is the thickness coordinate ($-\frac{h}{2} \leq z \leq \frac{h}{2}$). The plate's length, width, and total thickness are a, b, and h, respectively, Figure (7).

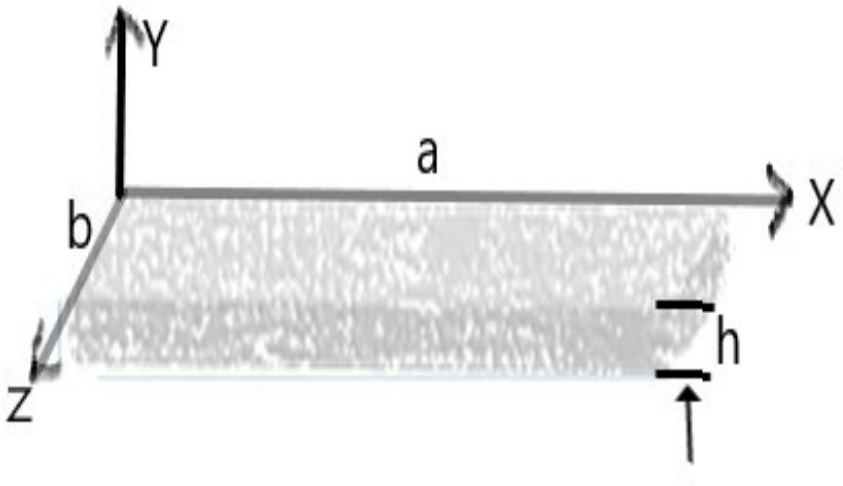

Figure 7 Geometry and coordinate system of the PFGB plate.

The material properties of P-FGB plates are written as [23] :

$$P(z) = (P_{PLA} - P_{UHMWPE})\left(1 + \frac{2z}{h}\right)^{n} + P_{UHMWPE} - P_{Por} \quad (6)$$

$$P_{Por} = \propto\backslash 2(1 - 2\left(\frac{|z|}{h}\right))(P_{PLA} + P_{UHMWPE}) \quad (7)$$

Accordingly, the effective Young's modulus $E(z)$, and the mass density ρ(z) of porous FGB plates can be written using Eq. (5):

$$\begin{bmatrix} E(z) \\ \rho(z) \end{bmatrix} = \begin{bmatrix} E_{PLA,UHMWP} \\ \rho_{PLA,UHMWP} \end{bmatrix} \left(1 + \frac{2z}{h}\right)^n + \begin{bmatrix} E_{UHMWP} \\ \rho_{UHMWP} \end{bmatrix} - \frac{\propto}{2}\left(1 - 2\left(\frac{|z|}{h}\right)\right) \begin{bmatrix} E_{PLA} + E_{UHMWP} \\ \rho_{PLA} + \rho_{UHMWP} \end{bmatrix} \quad (8)$$

Where α is the porosity distribution factor (porosity volume fraction), $E_{PLA,UHMWP} = E_{PLA} - E_{UHMWP}$, and $\rho_{PLA,UHMWP} = \rho_{PLA} - \rho_{UHMWP}$, the Poisson ratio ν(z) is assumed to be constant (ν(z)=ν), . Table (5) illustrates the mechanical properties of PFGBSs.

Table 5 The properties of PFGB.

Layers	Blend	Properties		
		Young's modulus E(MPA)	Poison's ratio	Density (g/cm^3)
Layers1	**PLA\UHMWPE\PVA5**	**43.6**	**0.27**	**1.108**

As shown in Figure (8, a, b), the composition of the interlayer is represented by the following power law equation:

$$C = (X/d)^P \quad (9)$$

where C is the volume fraction variations of the PLA and UHMWPE phases, d is the thickness of the interlayer, X is the distance from the PLA phase, and p is a numerical constant related to phase distribution or compositional gradient. The properties of the interlayer material are estimated assuming their linear dependencies on composition. Figure (8, a) shows the behavior of PLA\UHMWPE layers that behaves linearly and gradually with increasing volume fraction of the consistent of blends, and curing begins to rise.

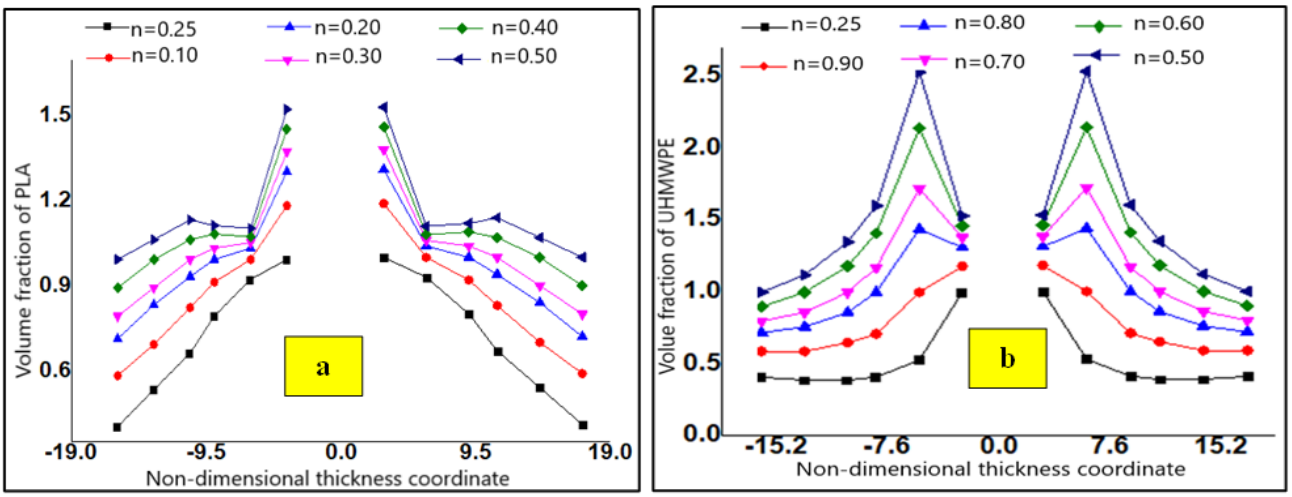

Figure 8 FGBs phase distribution profiles with varying power-law exponent: (a) V_{PLA} and (b) V_{UHMWPE} vs. non-dimensional thickness.

2.4.4 Finite element model for FGBs

Finite element models depict the components of functionally graded material layers to study their matrix exchange relationships and the factors affecting their failure. To understand and predict the influence of material, as well as geometric parameters, on the mechanical behavior of flexible composites filled with functionally graded matrices, finite element investigation may be a very feasible strategy. To achieve this, a simple discrete model (ANSYS 16) represents a model of FGB composites with properties varying from the porous top layer to the graded base. In this analysis, a three-dimensional model of the FGB system is constructed, as shown in Figures 9 (a) and 9 (c), and then meshed, as shown in Figures 9 (b) and 9 (d).

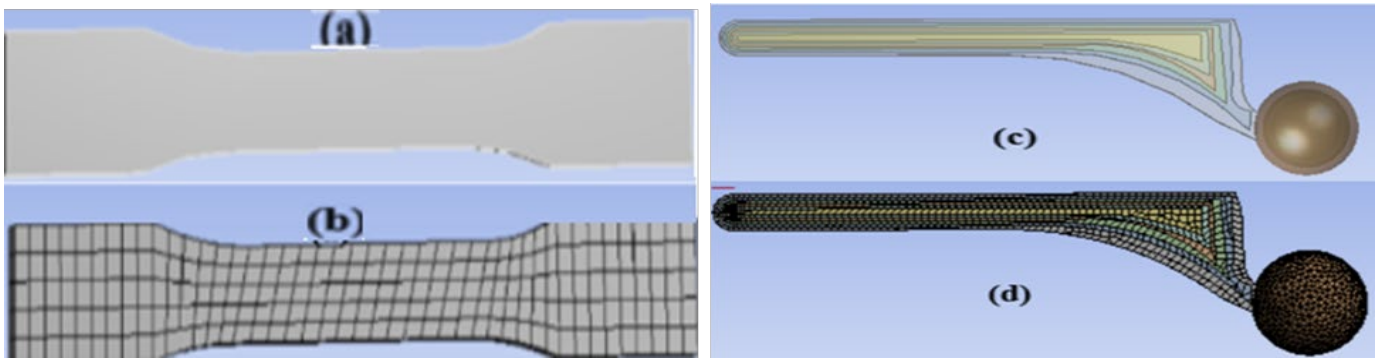

Figure 9 Three-dimensional model of (a) Tensile test sample, (b) Meshed Tensile sample, (c) FGB system sample, and (d) Meshed FGB system sample.

Finite element amounts are contrasted and test ones for tensile tests of functionally graded materials. Figure (9, a) indicates FE model with boundary conditions for tensile test investigation, total length (165 mm), gage length (57 mm), thickness of (3) mm (each layer of FGB with number of nodes (10010) and, number of elements (7384)), Figure (9, b). Moreover, Figure (9, c) the nodes are integrated at the interface permitting appropriate coupling amongst layers and interfaces for FGBs with total length (145mm) for stem prosthesis, diameter (32 mm) for ball head [24], number of nodes (6221), and number of elements (7045), Figure (9, d). The mesh is optimized for the prosthetic limb stump model as well as the loading models under tensile conditions because mesh optimization affects the accuracy of the results [25]. The Poisson's ratio and elastic modulus of FGBs are defined at a variety of weight fractions of (PLA, UHMWPE, and PVA) from experiments (tensile test), and are given as input to FEA as shown in table (3). The results obtained from the ANSYS program are as shown in Figure (10, a, b).

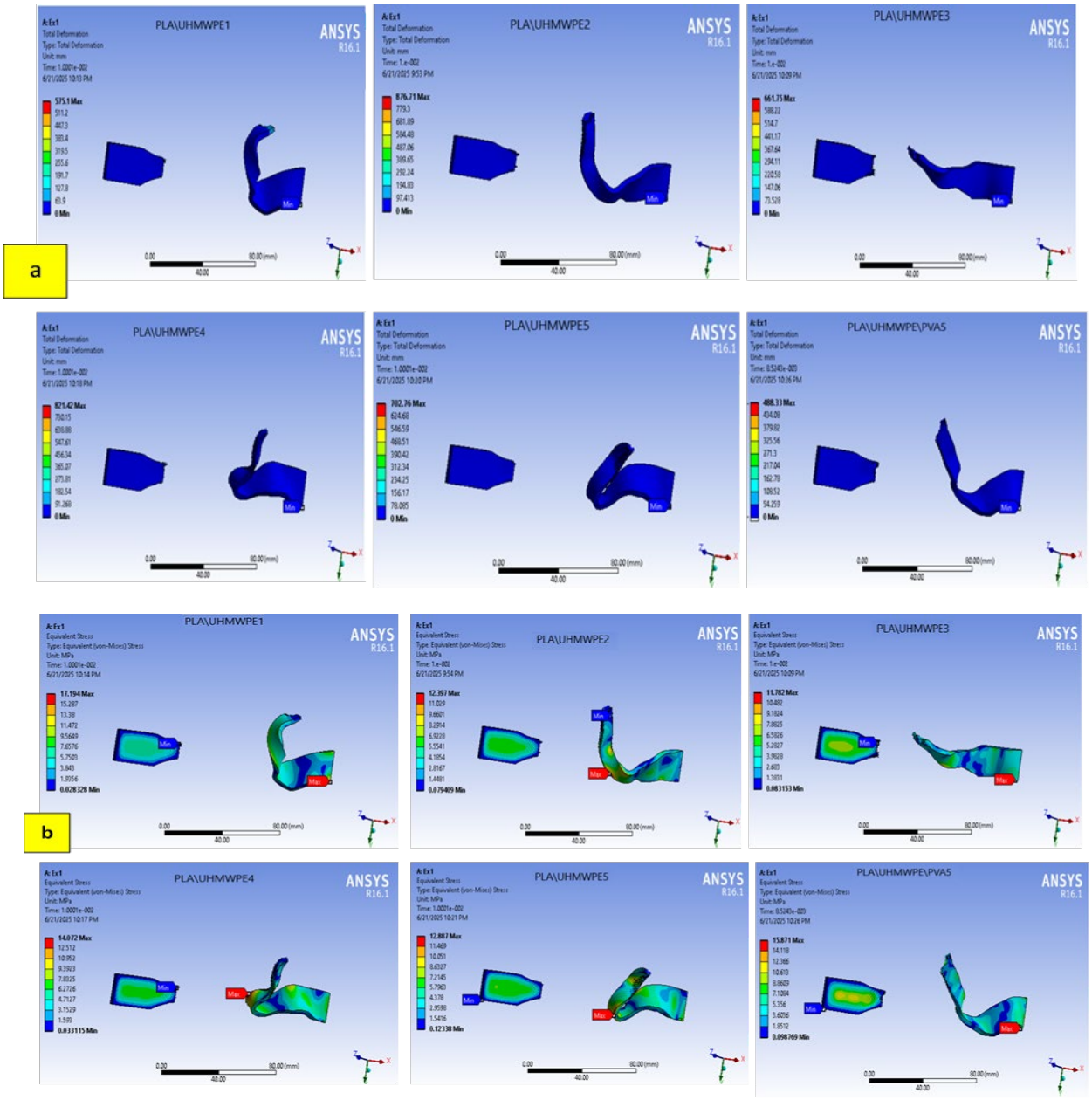

Figure 10 Numerical simulation results of the FGBs model: (a) total deformation and (b) equivalent stress.

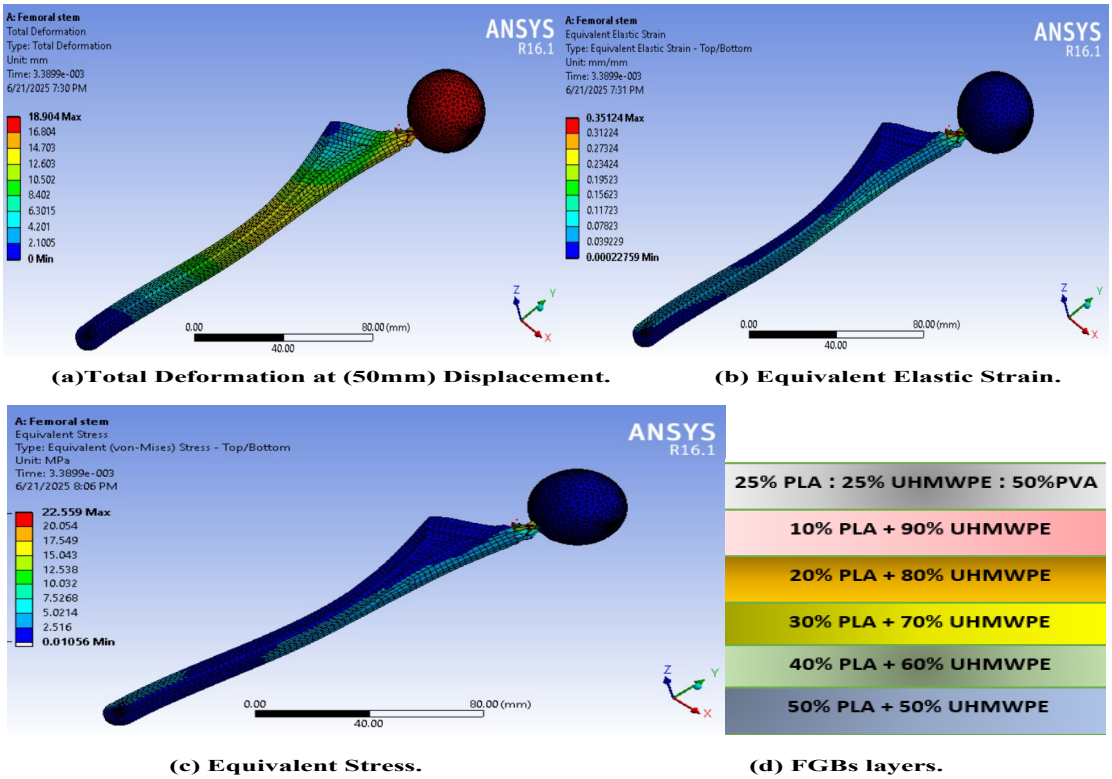

(a)Total Deformation at (50mm) Displacement. **(b) Equivalent Elastic Strain.**

(c) Equivalent Stress. **(d) FGBs layers.**

Figure 11 Prosthetic Stem Model Results Obtained From: Numerical Simulation (a), (b), (c), and (d) Illustration of the arrangement of FGB layers.

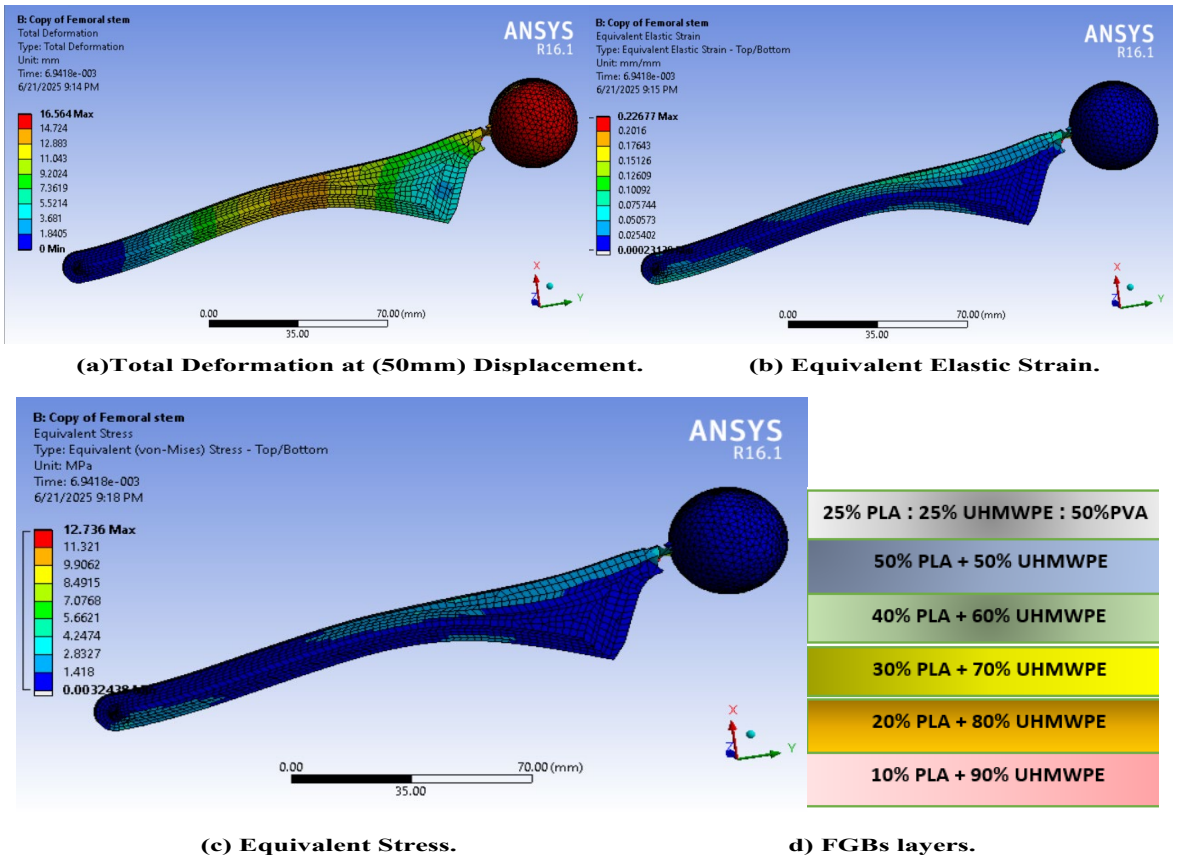

Figure 12 Prosthetic Stem Model Results Obtained From: Numerical Simulation (a), (b), (c), and (d) Illustration of the arrangement of FGB layers.

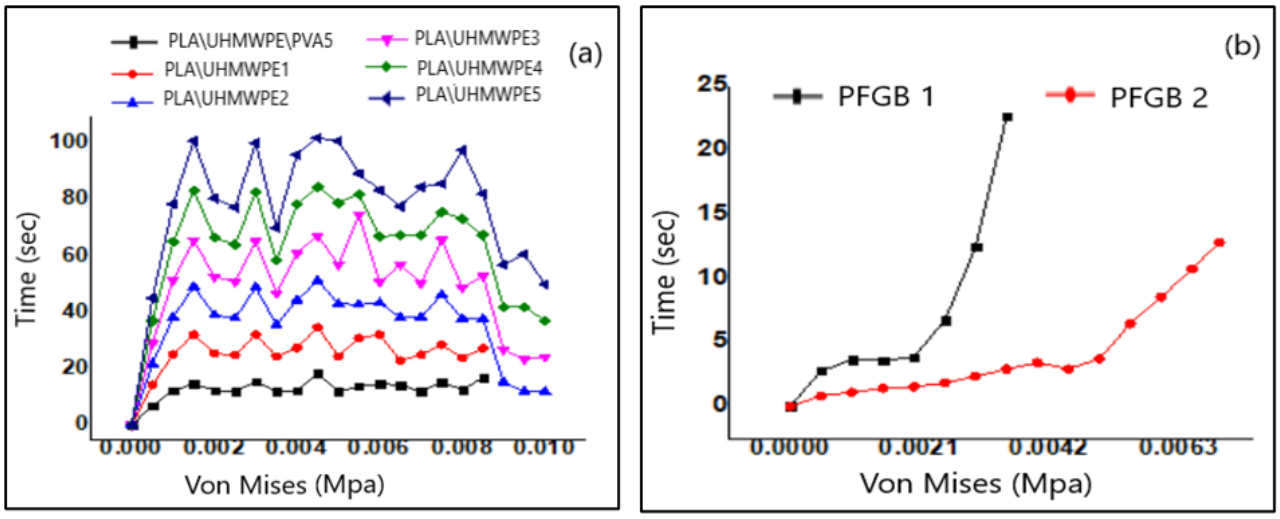

Figure 13 Diagram illustrating various profiles for: (a) PFGBs layer under Von-Mises stress, and (b) PFGB1 (Bottom-up hardness values), PFGB2 (Up-bottom hardness values).

4. RESULTS AND DISCUSSION

Figure (10, a, b) shows the variation in mechanical properties of heterogeneous mixtures associated with the composition (PLA, UHMWPE and PVA) under tensile conditions, by fixing the distal end of the test specimen and the lower leg to the artificial leg model and applying a displacement (40 mm) in the opposite direction to the fixation areas in both models (test specimen and leg). Describing the situation is often very difficult due to the change in blend properties depending on the controlling conditions. The lowest total deformation and highest von Mises stress values can be observed for blends (PLA\UHMWPE1, PLA\UHMWPE\PVA 5), which makes them more ductile. This indicates that the predominant phase is the high molecular weight polyethylene phase that surrounds the matrix, it's elastic and ductile properties prevail under tension. The highest total deformation and lowest stress are found in blends (PLA\UHMWPE 2, PLA\UHMWPE 3, PLA\UHMWPE4, and PLA\UHMWPE 5), which are less ductile. Here, the volume fractions gradually change with slight variation in von Mises stress values. This indicates that the similarity of volume fraction values creates a more cohesive structure that combines the properties of the two components, as discussed previously in the hardness and tensile testing sections.

Figures 11(a, b) and 12(a, b) show the artificial prosthetic stem models under tensile loading with different FGB stiffness gradients. In Figure 10, the gradient increases from the lowest (39.08) to highest (46.9). Maximum tensile force caused dislocation and loosening at the ball-head–stem interface, with total deformation of 16.564 mm and von Mises stress of 12.736 MPa at 50 mm displacement. In Figure 11, the gradient decreases from the highest (46.9) to lowest (39.08), resulting in similar interfacial dislocation under maximum load, with higher deformation (18.904 mm) and von Mises stress (22.559 MPa). These effects arise from the functionally graded nature of the FGBs, which feature uneven mechanical properties across layers, producing non-uniform stress and strain distributions. Interfaces between layers, often less stiff than the bulk, become critical points under tensile loading. Differences in Young's modulus across layers further amplify localized stress, leading to dislocation and loosening at the interface under maximum tensile load. This highlights the importance of gradient design in optimizing the mechanical performance of functionally graded prosthetic stems.

Figure (13, a) shows that each layer's behavior is similar to its behavior during the experimental test. Compare Figure (13, a) with Figure (6, a), where the surface porous layer has the highest deformation at the lowest time and stress, compared to the remaining layers, where stress concentrations vary depending on the amount of time required to reach failure and the volume fraction of the mixture components. Figure (12, b) shows the difference in three-dimensional stress when the layers are arranged according to the highest stiffness value after the porous layer. The model has higher deformation values than the model whose layers are arranged according to the lowest stiffness value after the porous layer. In general, the use of a mixture of two polymers with mechanical properties close to the bone enhances the transfer of load from the adjacent area to the distal area [25]. In particular, the use of PLA and UHMWPE with different volume fractions allows the structure to be designed based on the properties of actual bone, such that at maximum stress, the stem structure maintains its properties. However, the tensile strength has a significant effect on the bearing head, attributed to the loss of mass due to stress shielding and also sensitive to the design [26], material used [27], volume fraction exponent [28]. The most important error ratios for both the laboratory experimental results and the results obtained from for all PFGB layer are listed in the Table 6, are written as[29]:

$$\text{Errors} = \frac{Experimentally - Theoretically}{Experimentally} \quad (10)$$

Table 6 Errors ratios between experimental and analytical test for PFGB.

PLA\UHMWPE1	PLA\UHMWPE2	PLA\UHMWPE3	PLA\UHMWPE4	PLA\UHMWPE5	PLA\UHMWPE\PVA5
45%	43%	43%	55%	35%	39%

5. CONCLUSIONS

This research focused on the feasibility of using FGBP as a selective material for the production of prosthetic limb stems. The study focused on studying the deformation and stress mechanisms, revealing the strength of the selected materials, and revealing the unique properties of each material under loads, both experimentally and using finite element theory. The deformation and stress mechanisms of the prosthetic limb stem were also applied analytically. The study reported results showing that under tensile conditions, when the prosthetic leg model structure (PFGBs) takes a gradient according to stiffness values from the lowest (39.08) to the highest (46.9), dislocation and loosening are observed at the maximum tensile force at a displacement of (50 mm), the highest total deformation of (16.564 mm), and the maximum von Mises stress of (12.736 MPa). While the prosthetic leg model is under tension. While when the PFGBs structure takes a gradient according to stiffness values from the highest (46.9) to the lowest (39.08), dislocation and loosening occur at the maximum tensile force and at the point of contact of the ball head with the stem under tensile loading conditions at a displacement of (50 mm) for the highest total deformation of (18.904 mm) and a maximum von Mises stress of (22.559 MPa). A major limitation of this study is the lack of in vivo biomechanical loading [30][31]. The laboratory results of the tensile test were largely consistent with the analytical results obtained from the application of finite element theory. The load transfer mechanism at the point of contact plays a crucial role. If the load is not distributed evenly due to gradient formation, this can lead to higher stress concentrations at the interface. Softer layers exhibit localized elastic-plastic behavior, meaning that the UHMWPE phase predominates, while softer layers (with a higher PLA content) may not deform plastically. Similar volume fraction values create a more cohesive structure that combines the properties of both components. The addition of PVA has been shown to reduce mechanical properties, increase the compatibility of the blend[32][33], and impart texture to the matrix due to its hydrophilic properties and biodegradability, making it more suitable for engineering applications. Finally, we hope that future steps of this study will include the behavior of the material under real physiological or anatomical conditions (in vivo), to ensure the suitability of the study for application.

References

[1] J.M. Hatamzadeh, Y. Omidi, Prog. Polym. Sci. 47 (2015) 26 0.1002/pi.1887
[2] H.Z. A., Y.L. Xie, Y.X. Wang, L.P. Mo, Y.Y. Yang, Z.Y. Zhang, Mater. Chem. Phys. 114 (2009) 990 10.1201/9781003509523-1
[3] K.G. Adhikari, P. Cass, M. Bown, P. Gunatillake, RSC Adv. 5 (2015) 37553 https://doi.org/10.1039/D0RA07800J
[4] Z.Q. Cheng, F. Wang, Z. Chen, Y. Jiang, Z. Zhong, IEEE Int. Conf. Autom. Sci. Eng. (2015) 15 10.1088/1361-665X/ace66c
[5] Z.J. Guo, H. Xu, B. Cao, ACS Appl. Mater. Interfaces 5 (2013) 7893 https://doi.org/10.1002/adfm.202206900
[6] Israa Abdulqasim Mohammed Ali, Wafaa Hikmat Wadee, Kamal Mohammed Abood, Exp. Theo. NANOTECHNOLOGY 9 (2025) 423 https://doi.org/10.56053/9.S.423
[7] F.G. F. Cavanagh, L.M. Cavanagh, A. Afonja, R. Binions, Sensors 10 (2010) 5469 https://doi.org/10.1038/s41598-017-00891-5

[8] K.F. Wang, J. Zhang, H. Xia, B. Zhu, Y. Wang, S. Wu, Mater. Sci. Eng. B 150 (2008) 6 https://doi.org/10.3390/s100605469
[9] D.A. Manurung, R.V. Asri, L.A. Yuliarto, B. Nugraha, N. Nugraha, B. Sunendar, Indones. J. Chem. 18 (2018) 344 https://doi.org/10.1016/j.jma.2020.02.003
[10] N.M. Abdullah, N. Demon, S.Z.N. Halim, I.S. Mohamad, Polymers 13 (2021) 1916 10.1088/1402-4896/ac4943
[11] W.F. Gu, T.M. Swager, J. Am. Chem. Soc. 130 (2008) 5392 10.1039/c1cc11517k
[12] M.A. Salam, M.S. Makki, M.Y. Abdelaal, J. Alloys Compd. 509 (2011) 2582 https://doi.org/10.1016/j.jmrt.2022.03.099
[13] H.A. Ahmad, F. Mohammad, Materialia 14 (2020) 100868 https://doi.org/10.30723/ijp.v22i4.1181
[14] J.G.V. Rajendran, Mater. Lett. 139 (2015) 116 10.3390/biom9100611
[15] W.F. Gu, T.M. Swager, J. Am. Chem. Soc. 130 (2008) 5392 https://doi.org/10.1021/cm102406h
[16] Marwa Sulaiman, Enas Muhi Hadi, Exp. Theo. NANOTECHNOLOGY 9 (2025) 431 https://doi.org/10.56053/9.S.431
[17] M. Trifkovic, A. Hedegaard, K. Huston, M. Sheikhzadeh, C.W. Macosko, Macromolecules 45 (2012) 6036 10.1021/ma300293v
[18] M. Trifkovic, A.T. Hedegaard, M. Sheikhzadeh, S. Huang, C.W. Macosko, Macromolecules 48 (2015) 4631 https://doi.org/10.1021/ma020754t
[19] Zainab Naseer Hasheem, Estabraq Talib Abdullah, Experimental and Theoretical NANOTECHNOLOGY 9 (2025) 303 https://doi.org/10.56053/9.S.303
[20] N.R. Washburn, C.G. Simon Jr., A. Tona, H.M. Elgendy, A. Karim, E.J. Amis, J. Biomed. Mater. Res. 60 (2002) 20 https://doi.org/10.1002/jbm.a.30054
[21] Rana A. Anaee, Rana A. Anaee, Marwa A. Abbas, Saja A. Abdul Maged, Shaimaa A. Naser, Sinan S. Hamdi, Hussain M. Yousif, Nabil J. AL-Bahnam, Tamara A. Anai, Exp. Theo. NANOTECHNOLOGY 9 (2025) 449 https://doi.org/10.56053/9.S.449
[22] K. Foroutan, A. Shaterzadeh, H. Ahmadi, Appl. Math. Model. 77 (2020) 539 https://doi.org/10.1016/j.apm.2019.07.062
[23] Y. Torres, J. Trueba, A. Cabezas, J. Pavón, F.J. Gil, Mater. Des. 110 (2016) 179 https://doi.org/10.1016/j.matdes.2016.07.135
[24] Sundus A. Abdullah Albakri, Aya F. Ibrahim, Hawraa A. Hussein, Experimental and Theoretical NANOTECHNOLOGY 9 (2025) 311 https://doi.org/10.56053/9.S.311
[25] S. Huzni, M.I. Tanamas, S. Fonna, A.K. Ariffin, IOP Conf. Ser. Mater. Sci. Eng. 931 (2020) 012001 10.1088/1757-899X/602/1/012086
[26] M. Ceddia, G. Solarino, G. Giannini, G. De Giosa, M. Tucci, B. Trentadue, J. Compos. Sci. 8 (2024) 254 https://doi.org/10.3390/jcs8070254
[27] H.S. Hedia, N. Fouda, Mater. Test. 55 (2013) 23 https://doi.org/10.3139/120.110400
[28] V.T. Van, N.H.T. Tai, N.N. Hung, J. Sci. Technol. Civ. Eng. 15 (2021) 141 https://doi.org/10.1142/S0219455425502360
[29] Rusul Adnan Al-wardy, Experimental and Theoretical NANOTECHNOLOGY 9 (2025) 327 https://doi.org/10.56053/9.S.327
[30] S. Wachirahuttapong, C. Thongpin, N. Sombatsompop, Energy Procedia 89 (2016) 198 https://doi.org/10.1016/j.egypro.2016.05.026
[31] J.W. Park, D.J. Lee, E.S. Yoo, S.S. Im, S.H. Kim, Y.H. Kim, Korea Polym. J. 7 (1999) 93 https://doi.org/10.1007/BF03218391
[32] Ahmed S. Hassan, Jasim H. Kadhum, Sarmad Najah ALSalhy, Osama T. Al-Taai, Experimental and Theoretical NANOTECHNOLOGY 9 (2025) 335 https://doi.org/10.56053/9.S.335
[33] Y. Hu, Q. Wang, M. Tang, Carbohydr. Polym. 96 (2013) 384 https://doi.org/10.3390/molecules28145416

Exp. Theo. NANOTECHNOLOGY 10 (2026) 109-121